ACS Sustainable Chemistry & Engineering

Research Article

Cite This: ACS Sustainable Chem. Eng. XXXX, XXX, XXX−XXX

pubs.acs.org/journal/ascecg

Nitrogen-Doped Hollow Mesoporous Carbon Spheres Modified g-C_3N_4/Bi_2O_3 Direct Dual Semiconductor Photocatalytic System with Enhanced Antibiotics Degradation under Visible Light

Binbin Shao,[†] Zhifeng Liu,*[,†] Guangming Zeng,*[,†] Zhibin Wu,[‡] Yang Liu,[†] Min Cheng,[†] Ming Chen,[†] Yujie Liu,[†] Wei Zhang,[†] and Haopeng Feng[†]

[†]College of Environmental Science and Engineering, Hunan University and Key Laboratory of Environmental Biology and Pollution Control (Hunan University), Ministry of Education, South Lushan Road, Yuelu District, Changsha 410082, PR China

[‡]College of Bioscience and Biotechnology, Hunan Agricultural University, Nongda Road, Furong District, Changsha 410128, PR China

Supporting Information

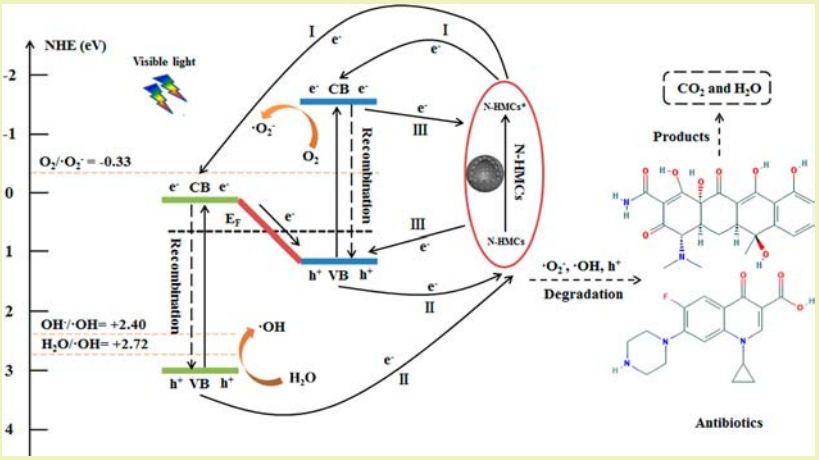

ABSTRACT: Herein, the nitrogen-doped hollow mesoporous carbon spheres (N-HMCs) modified g-C_3N_4/Bi_2O_3 direct dual semiconductor photocatalyst (g-C_3N_4/Bi_2O_3@N-HMCs) were synthesized by a facile thermal process. The morphology, structure, elements, and photoelectrochemical properties of the as-prepared samples were characterized by electron microscopy, N_2 sorption−desorption, X-ray diffraction, X-ray photoelectron spectroscopy, diffuse-reflectance spectra, and photoluminescence spectroscopy, among other technologies. The photocatalytic efficiency was evaluated toward degradation of antibiotics tetracycline hydrochloride (TCH) and ciprofloxacin hydrochloride (CFH) under visible-light irradiation, and the results showed that the g-C_3N_4/Bi_2O_3@N-HMCs composite exhibited superior photocatalytic efficiency than other comparison samples, which could be attributed to the synergistic action of g-C_3N_4/Bi_2O_3 direct dual semiconductor photocatalytic system and the N-HMCs. The characterization techniques revealed that N-HMCs play three vital roles in improving photocatalytic efficiency. First, N-HMCs could serve as a photosensitizer to enhance visible-light absorption. Second, N-HMCs are an excellent conductive material to transfer the photoexcited electrons quickly to hinder the electron−hole pairs recombination. Third, N-HMCs could provide more active sites in the photocatalytic process. The scavenger experiments and electron-spin-resonance results revealed that the active substances h^+, $^{\bullet}O_2^-$, and $^{\bullet}OH$ performed together in the photodegradation system. Additionally, the g-C_3N_4/Bi_2O_3@N-HMCs composite showed favorable photostability after six rounds of recycling, suggesting the great prospects of the practical application of g-C_3N_4/Bi_2O_3@N-HMCs.

KEYWORDS: *g-C_3N_4/Bi_2O_3@N-HMCs, Direct dual semiconductor photocatalytic system, Electron transfer, Antibiotics, Visible photocatalytic degradation*

INTRODUCTION

Over the past few decades, the overuse and incomplete metabolism of antibiotics have caused serious environmental pollution, which could interfere with the growth of living cells and promote the proliferation of antibiotic-resistant pathogens.[1−3] Many studies have focused on the removal of antibiotic contaminants, such as filtration, adsorption, biodegradation, semiconductor photocatalysis, and so on.[4−8]

Received: July 19, 2018
Revised: September 12, 2018
Published: October 10, 2018

DOI: 10.1021/acssuschemeng.8b03480
ACS Sustainable Chem. Eng. XXXX, XXX, XXX−XXX

Among these studies, semiconductor photocatalysis can be a promising remediation technology which can be applied to remove various organic or inorganic contaminants in an ecofriendly and high-efficiency way.[9]

In 1972, Fujishima and Honda[10] first reported that the semiconductor TiO_2 could photocatalyze water splitting into O_2 and H_2 under ultraviolet light (UV) irradiation. Nowadays, many semiconductor-based photocatalysts have been investigated for energy and environmental protection,[11] such as metallic (composite) oxide, metal (composite) sulfide, and some nonmetal materials.[12,13] Metal-free graphite C_3N_4 (g-C_3N_4) especially has recently gained great interest due to the favorable photocatalytic efficiency under visible-light irradiation. g-C_3N_4 is a delocalized conjugative π structure polymer semiconductor, which could be facilely prepared by pyrolysis of melamine, dicyandiamide, or urea.[13,14] Generally, the conduction band (CB) and valence band (VB) position of g-C_3N_4 are −1.13 and 1.57 eV, respectively. The appropriate band gap (2.70 eV) of g-C_3N_4 makes its favorably respond to visible light and is widely studied to solve the environmental problems and energy crises.[15] Nevertheless, the passive photocatalytic activity of the pristine g-C_3N_4 always occurs because of the rapid recombination of photoexcited electron−hole (e^-−h^+) pairs and the poor specific surface area.[16,17] For enhancing the photocatalytic activity of g-C_3N_4, multifarious strategies have been employed.[13] One effective strategy is combining g-C_3N_4 with other semiconductor materials to build a dual semiconductor photocatalytic system, which has roots in natural photosynthesis and is considered to be the most effective photocatalytic system.[18] The dual semiconductor photocatalytic system could be classified into two categories: dual semiconductor systems with solid-state electron mediators and those without redox-mediators as "direct dual semiconductor system".[19,20] Compare to the former, the latter possesses better-photogenerated charge carriers separation, higher light absorption, and so on.[20] To date, diverse direct dual semiconductor photocatalytic system about g-C_3N_4 have been constructed, such as Ag_3PO_4/g-C_3N_4,[21] V_2O_5/g-C_3N_4,[22] CoTiO3/g-C_3N_4,[23] BiOI/g-C_3N_4,[24] Bi_2MoO_6/g-C_3N_4,[25] and g-C_3N_4/Bi_2O_3,[26] among others.

Among semiconductor materials, Bi_2O_3 should be a promising candidate due to the excellent stability, outstanding optical properties, low/nontoxicity, and earth abundance.[9] To establish a direct dual semiconductor photocatalytic system, energy levels of the two semiconductors need to match.[18,26] Bi_2O_3 is a significant metal oxide semiconductor with the band gap near that of g-C_3N_4 (2.80 eV). The CB and VB positions of Bi_2O_3 are 0.33 and 3.13 eV, respectively.[4] Meanwhile, the photoexcited electron on g-C_3N_4 CB is negative enough to reduce O_2, generating $^{\bullet}O_2^-$ (the potential of O_2/$^{\bullet}O_2^-$ is −0.33 eV),[27] and the photoexcited hole on Bi_2O_3 VB is positive enough to oxidize H_2O or OH^- to $^{\bullet}OH$ (the potential of H_2O/$^{\bullet}OH$ and OH^-/$^{\bullet}OH$ are 2.72 and 2.40 eV, respectively).[22,26] So far, several studies have developed g-C_3N_4/Bi_2O_3 direct dual semiconductor photocatalyst.[26,28,29] Although the photocatalytic performance of the photocatalyst has been greatly improved compared with each pristine photocatalyst, the visible-light absorption, e^-−h^+ pairs separation efficiency, charge migration rate and available active site of g-C_3N_4/Bi_2O_3 heterojunction still need to be improved.[26,29]

To solve these issues, a common material, namely carbon spheres (CS) are often combined with the semiconductor because of their prominent conductivity, corrosion resistance, high specific surface area, and low price.[30−33] Zhao et al.[30] found that CS play a significant role in improving the photocatalytic activity of CuO-$BiVO_4$@CS heterojunction for mineralizing methylene blue. Wu et al.[33] prepared CS modified BiOI/$BiOIO_3$ composite and it exhibited much higher photocatalytic removal efficiency of gaseous Hg^0 than BiOI/$BiOIO_3$ composite under visible-light irradiation. These CS could serve as a photosensitizer to transfer electrons to the semiconductor, restraining the recombination of e^-−h^+ pairs and increasing the visible-light absorption, thus improving the photocatalytic efficiency of photocatalyst.[30−32,34] The nitrogen-doped hollow mesoporous carbon spheres (N-HMCs) can be a versatile CS due to the specific hollow core-mesoporous shell structure, high specific surface area, abundant pore volumes, excellent electric conductivity, and thermochemical stability.[35,36] The remarkable properties enable the N-HMCs great potential to be applied in many fields, such as energy storage/conversion, adsorption, and catalysis, and so on.[35,37−39] Unfortunately, to the best of our knowledge, there is a lack of investigation on the N-HMCs in the g-C_3N_4/Bi_2O_3 direct dual semiconductor photocatalytic system.

Herein, the N-HMCs modified g-C_3N_4/Bi_2O_3 direct dual semiconductor photocatalyst (g-C_3N_4/Bi_2O_3@N-HMCs) were prepared with enhanced visible-light-active toward degradation of antibiotics tetracycline hydrochloride (TCH) and ciprofloxacin hydrochloride (CFH). The structure, morphology, and optical properties of the obtained photocatalysts were characterized by XRD, XPS, FESEM, TEM, UV−vis DRS, PL, ESR, and so on. The photogenerated charge migration and separation of g-C_3N_4/Bi_2O_3@N-HMCs and the degradation mechanism of antibiotics were investigated. Moreover, the stability of the photocatalyst was also assessed through cyclic degradation experiments. It is expected that this photocatalyst could be a hopeful candidate for degrading environmental contaminants and applying in environmental remediation.

EXPERIMENTAL SECTION

Materials. Tetrapropyl orthosilicate (TPOS, purity > 97%) was purchased from Aladdin Industrial Corporation (Shanghai, China). Melamine, bismuth nitrate pentahydrate ($Bi(NO_3)_3{\cdot}5H_2O$), ammonium hydroxide ($NH_3{\cdot}H_2O$), formaldehyde, resorcinol, and thiourea were obtained from Sinopharm Chemical Reagent Co., Ltd. (Shanghai, China). TCH and CFH were purchased from Bomei Biological Technology Co., Ltd. (Hefei, China). All other chemicals were analytical-grade and used as received. The ultrapure water was used throughout the experiment with a resistivity of 18.25 MΩ cm^{-1}.

Synthesis of N-HMCs. N-HMCs (NHC) were prepared follows the previous report with some modification,[40] and the details were shown in the Supporting Information.

Synthesis of g-C_3N_4/Bi_2O_3@N-HMCs. To fabricate g-C_3N_4/Bi_2O_3@N-HMCs composite, in detail, a quantity of N-HMCs (0.024, 0.049, 0.100, 0.153, and 0.267 g), 4.5 g of melamine, and 0.5 g of $Bi(NO_3)_3{\cdot}5H_2O$ were placed together in a mortar and ground evenly. Then, the mixture was calcined at 550 °C (2.3 °C min^{-1}) under N_2 atmosphere for 4 h in a tube furnace. After natural cooling and grinding, samples with the different ratio of N-HMCs (1, 2, 4, 6, and 10%) were obtained, and they were labeled as CBH-1, CBH-2, CBH-4, CBH-6, and CBH-10, respectively. In the pre-experiment, these five CBH samples were used in the study of photodegradation of TCH; the results indicated that the best photocatalytic performance of CBH was obtained after doping 4% N-HMCs. Thus, 4% CBH was used for further study and characterization and written as CBH (see Figure S2). Therefore, the final theoretical composition of sample CBH included 4% N-HMCs, 9.6% Bi_2O_3, and 86.4% g-C_3N_4. For

DOI: 10.1021/acssuschemeng.8b03480
ACS Sustainable Chem. Eng. XXXX, XXX, XXX−XXX

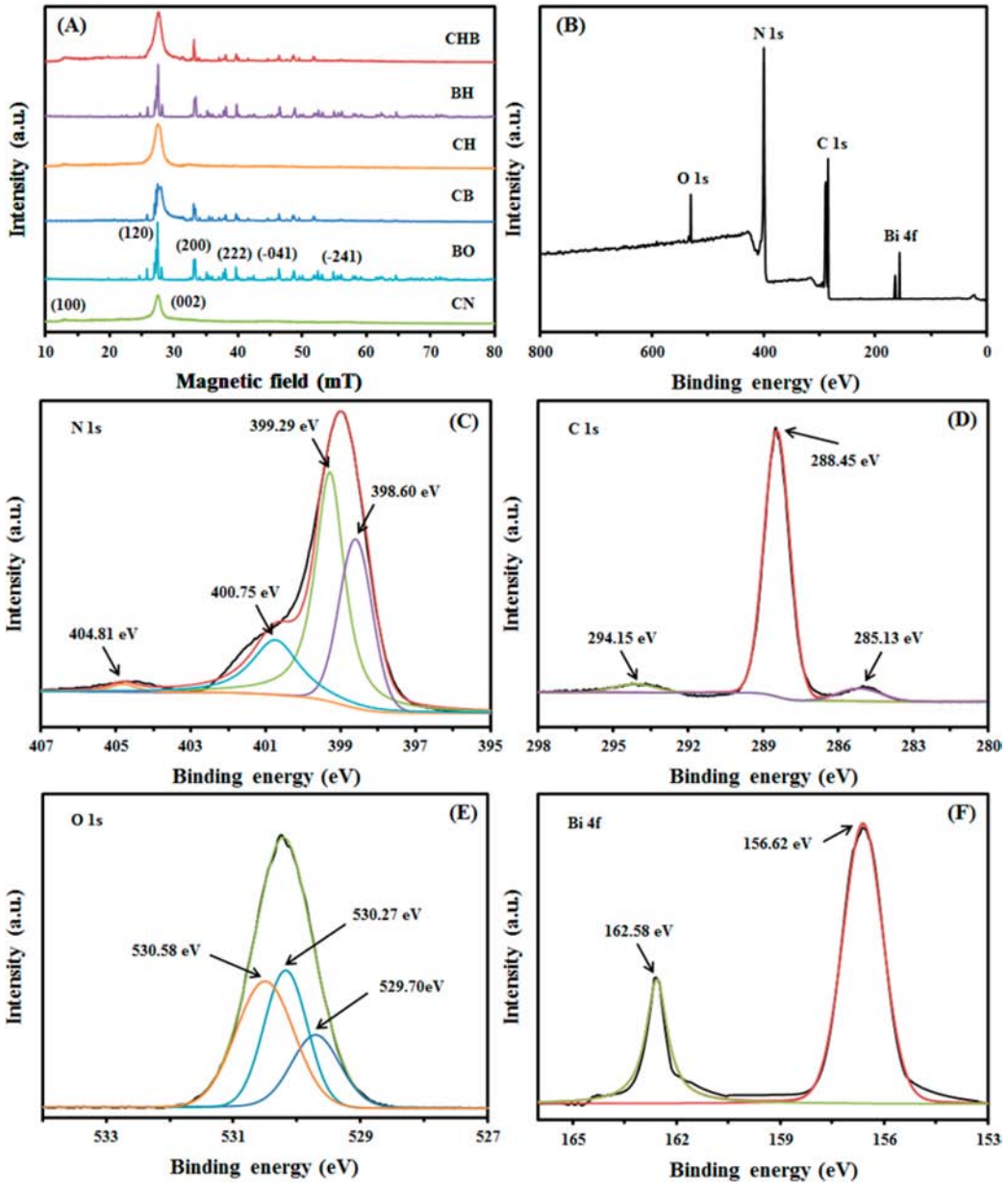

Figure 1. (A) XRD patterns of the as-prepared samples; (B) XPS spectra of the CBH composite. Survey of the samples: (C) N 1s; (D) C 1s; (E) O 1s; (F) Bi 4f.

comparison purposes, single-phase g-C_3N_4 (CN), single-phase Bi_2O_3 (BO), and binary composites (g-C_3N_4/N-HMCs (CH), Bi_2O_3/N-HMCs (BH), and g-C_3N_4/Bi_2O_3 (CB)) were synthesized by the same calcination method. Binary composites CH, BH, and CB were prepared with the same procedure without $Bi(NO_3)_3{\cdot}5H_2O$, melamine, and N-HMCs, respectively. CN and BO only used melamine and $Bi(NO_3)_3{\cdot}5H_2O$ as the precursor, respectively.

Characterization. The morphological structure of the samples was characterized by field-emission scanning electron microscopy (FESEM, FEI, Quanta-F250) and transmission electron microscopy (TEM, FEI, Tecnai-G2 F20). The crystal phase of the samples was determined by X-ray diffraction (XRD) using Cu Kα source. The surface elemental composition was detected by X-ray photoelectron spectroscopy (XPS, PHI5300, Japan) with the C 1s peak at 284.8 eV as the reference. The N_2 adsorption−desorption isotherms were measured on Quadrasorb SI analyzer at 77 K. The specific surface area, pore volume, and pore diameter were calculated based on Brunauer−Emmett−Teller (BET) analyses at the degassing temperature was 150 °C for 3 h. The UV−vis diffuse-reflectance spectra (UV−vis DRS) were equipped with an integrating sphere assembly using $BaSO_4$ as the reflectance standard. The photoluminescence (PL) spectroscopy was measured on Hitachi F-7000 fluorescence spectrophotometer at the excitation wavelength was 350 nm. The photoelectrochemical experiments were performed on an electrochemical workstation (CHI 660C, China) in a three-electrode system. The thermogravimetric analysis (TGA) was performed under air atmosphere from room temperature to 800 °C at a heating rate of 10 °C min^{-1} (TGA-Q600, USA). The electron-spin-resonance (ESR) signals were monitored on a Bruker spectrometer under visible-light irradiation (λ > 420 nm). The mineralization efficiency was examined by total organic carbon (TOC) measurements.

Photocatalytic Assessment. The photocatalytic behaviors of the as-prepared samples were estimated using 10 mg L^{-1} TCH and 10 mg L^{-1} CFH as a pollutant. In detail, 100 mg of sample was added to 100 mL of contaminant aqueous solution. Before irradiation, the suspension was stirred for 30 min in the dark; then, photocatalytic experiments were carried out under the visible-light irradiation using a 300 W xenon lamp as the light source (Beijing China Education Au-

DOI: 10.1021/acssuschemeng.8b03480
ACS Sustainable Chem. Eng. XXXX, XXX, XXX−XXX

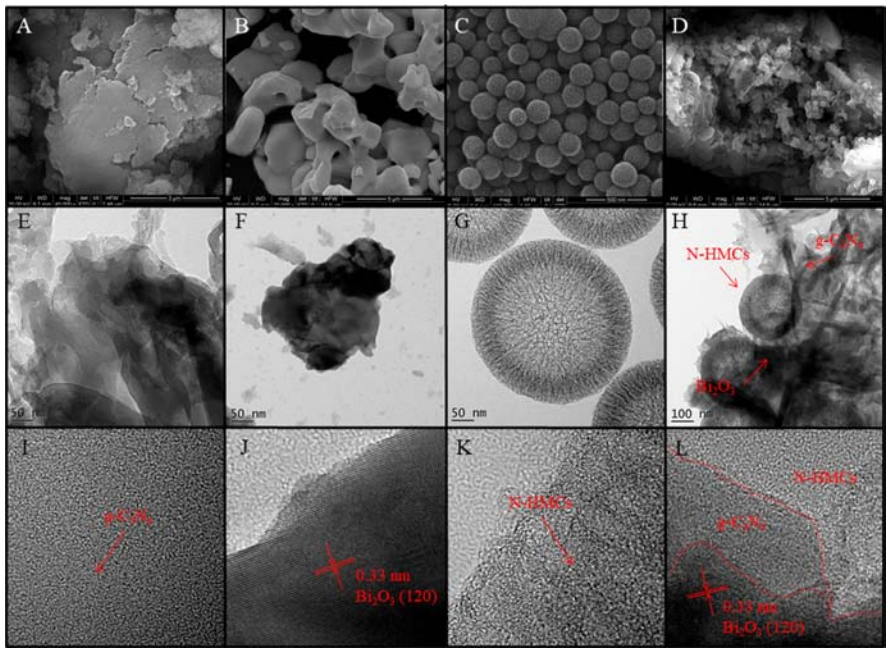

Figure 2. SEM images of CN (A), BO (B), N-HMCs (C), and CBH (D). TEM images of CN (E), BO (F), N-HMCs (G), and CBH (H). HRTEM images of CN (I), BO (J), N-HMCs (K), and CBH (L).

light, Co., Ltd., $\lambda > 420$ nm). (On the basis of the results of the long-time adsorption experiment, the adsorption−desorption equilibrium was reached after 30 min; see Figure S3.) At every 10 min interval, 1.0 mL of the suspension was withdrawn and then filtrated for analysis. The concentrations of TCH and CFH were detected through an UV−vis spectrophotometer at the characteristic absorption peak of 357 and 275 nm, respectively.

RESULTS AND DISCUSSION

Crystal Structure, Chemical States, Morphology, And Thermal Stability. The crystal structure and composition of the as-prepared samples were characterized by XRD. As displayed in Figure 1A, the peaks of single-phase g-C_3N_4 at 2θ values of 13.21 and 27.2° could be attributed to (100) and (002) crystal planes (Powder Diffraction File (PDF) no. 87−1526, Joint Committee on Powder Diffraction Standards (JCPDS), [2004]), respectively, which represented the typical graphitic-like layered stacking of CN-based materials.[4] For single-phase Bi_2O_3, all peaks corresponded well to the standard monoclinic phase α-Bi_2O_3 (PDF no. 41−1449, JCPDS, [2004]),[41] and the sharp diffraction peaks of Bi_2O_3 indicated the good crystallinity. Two binary samples, namely, CH and BH, showed the similar XRD patterns to single-phase g-C_3N_4 and Bi_2O_3, respectively. It indicated that the introduction of N-HMCs into the photocatalyst had no significant effect on the crystalline nature. In contrast, the peak at 2θ = 27.2° seemed even stronger; it could be that the graphite structure also exists in N-HMCs.[42] As shown in Figure S4, two peaks located at 25.4 and 42.3° were observed, which could be attributed to typical graphitic (002) and (100) planes, respectively.[30] For binary sample CB, it is obvious that the characteristic peaks of each component had been contained. Moreover, the XRD pattern of CBH composite is similar to that of CB, but the diffraction peak at a 2θ value of 27.2° seemed even stronger, which indicated that the CBH composite was formed with no other impurities.

The surface chemical states of the CBH sample were characterized through XPS; the spectrograms were depicted in Figure 1. The XPS survey spectra (Figure 1B) displayed that the predominant elements of the CBH composite were N, C, O, and Bi. Moreover, the high-resolution XPS spectra of N 1s, C 1s, O 1s, and Bi 4f were exposed. According to Figure 2C, the N 1s spectra could be decomposed into four characteristic peaks with binding energies at 398.60, 399.29, 400.75, and 404.81 eV. The peaks at 398.60 and 404.81 eV corresponded to C−N═C species and positive charge localization, respectively.[43] The peak at 399.29 and 400.75 eV were assigned to N−$(C)_3$ groups and C−N−H bonds, respectively.[44] Figure 2D displayed the high-resolution spectra of C 1s; the peak at 285.13 and 288.45 eV could be assigned to sp^2 bonded carbon (C−C) and sp^2 hybridized carbon in N-containing aromatic ring (N−C═N) from g-C_3N_4, respectively.[45,46] The peak at 294.15 eV could be assigned to the surface absorbed function groups (C═O).[47] As to the O 1s (Figure 2E), the peak at 529.70 eV is associated with the O^{2-} in the Bi_2O_3.[48] The peaks at 530.58 and 530.27 eV may be attributed to the absorbed H_2O molecule and hydroxyl group on the surface of CBH composite.[24] For Bi 4f, as shown in Figure 2F, the Bi 4f XPS spectrum could be divided into two characteristic peaks with the binding energies of 156.62 and 162.58 eV, which could be assigned to Bi $4f_{7/2}$ and Bi $4f_{5/2}$, respectively.[49] Moreover, the XPS spectrum of g-C_3N_4 was also supplied (Figure S5); the results indicated that the carbon content in g-C_3N_4 was 41.15 atom %. However, the carbon content in CBH was 45.08 atom % (Table S2), which confirmed the N-HMCs were successfully incorporated into the CBH. Therefore, these results indicated the coexistence of g-C_3N_4, Bi_2O_3, and N-HMCs in the CBH composite.

The FESEM, TEM, and HRTEM technologies were applied to study the morphological structure of the as-prepared samples. According to the SEM images (Figure 2A−D), the g-C_3N_4 sample exhibited platelike, stacked sheets, and smooth surface (Figure 2A), which is the representative structure feature of g-C_3N_4 prepared by thermal treatment technique.[16] From Figure 2B, it is obvious that the Bi_2O_3 was blocky, with

DOI: 10.1021/acssuschemeng.8b03480
ACS Sustainable Chem. Eng. XXXX, XXX, XXX−XXX

sharp edges and a smooth surface; the particle size of $Bi_2O_3$was about 265 nm. As shown in Figure 2C, the N-HMCs were a uniform sphere, with many open entrances distributed on the surface. According to the measurement, the average diameter of N-HMCs was about 330 nm, and the thickness of the shell was about 40 nm. As for the CBH composite (Figure 2D), it could be seen that the three materials are bound together firmly and that the N-HMCs and Bi_2O_3 coated on the surface of bulk g-C_3N_4. The element mapping also showed that the CBH sample consists of uniformly distributed elements of C, N, O, and Bi elements (Figure S6). Besides, the TEM figures (Figure 2E−H) showed more details of the as-prepared samples. According to Figure 2E,F, the g-C_3N_4 had a stacked sheets structure, and Bi_2O_3 had a nanoparticle structure, respectively. Figure 2G confirmed that the N-HMCs had a hollow morphology, with many pore channels distributed over the shell. Interestingly, it is obvious that the N-HMCs and Bi_2O_3 were randomly attached on g-C_3N_4 (Figure 2H). The results obtained from TEM images were consistent with the results of SEM images. High-resolution TEM (HRTEM) was further performed to explore the detailed crystal structure of the as-prepared samples. As displayed in Figure 2I,K, pure g-C_3N_4 and N-HMCs exhibited amorphous structures.[4,30] However, the lattice spacing of 0.33 nm corresponds to the (120) plane of Bi_2O_3 (Figure 2J).[4] As for the CBH composite (Figure 2L), there is obvious coexistence of g-C_3N_4, N-HMCs, and Bi_2O_3 phases, which further confirmed that the CBH composite was successfully synthesized.

The specific surface area and pore features of g-C_3N_4, Bi_2O_3, N-HMCs, and CBH samples were investigated by N_2 sorption analysis. The N_2 sorption isotherms and pore diameter distributions of the samples were shown in Figure S7. Clearly, all samples followed the type-IV isotherm with an H3 hysteresis loop, which indicated that the samples had a mesoporous structure.[26] Meanwhile, the pore diameter distributions further showed that the mesoporous exist in the samples. The BET surface area, pore volume, and average pore diameter of the four samples were listed in Table 1. It was

Table 1. Pore Structure Parameters of BO, CN, NHC, and CBH

sample	BET surface area ($m^2\ g^{-1}$)	pore volume ($cm^3\ g^{-1}$)	average pore diameter (nm)
BO	1.067	0.001	14.361
CN	7.883	0.012	15.214
NHC	518.6	0.993	13.836
CBH	18.75	0.109	21.208

interesting that the values of BET surface area, pore volume, and average pore diameter of N-HMCs were 518.6 $m^2\ g^{-1}$, 0.993 $cm^3\ g^{-1}$, and 13.936 nm, respectively. The excellent structure properties of N-HMCs could be caused by the hollow core−mesoporous shell structure. However, compared to the N-HMCs, three other samples showed poor specific surface area and porous structure. Fortunately, the CBH composite possesses much higher BET surface area (18.750 $m^2\ g^{-1}$), pore volume (0.109 $cm^3\ g^{-1}$), and average pore diameter (21.202 nm) compared with those of single-phase g-C_3N_4 and Bi_2O_3, these results could result from the introduction of N-HMCs (Table 1). The superior surface and structural properties of the photocatalyst will provide more active sites and cause more contaminants to adsorb on its surface.

TGA was performed for investigating the thermal stability of the samples. As shown in Figure 3A, pure Bi_2O_3 showed excellent thermal stability; there is almost no weight loss throughout the thermal process. For g-C_3N_4, a sharp weight loss occurred from 530 to 750 °C, which could be attributed to the burning of g-C_3N_4.[29] For N-HMCs, two weight loss processes, namely, from 110 to 240 °C and from 460 to 630 °C, which could be assigned the loss of surface absorbed water and N-HMCs burning. As for the CBH composite, the weight loss mainly happened from 480 to 710 °C; this was due to the presence of g-C_3N_4 and N-HMCs. g-C_3N_4 was the main component of CBH. Meanwhile, there was about 10.5% substance still existing, which should be composed of Bi_2O_3 and some others residues; this result is consistent with the above calculation, namely, the content of Bi_2O_3 was 9.6% in the CBH composite.

Optical Properties. The optical absorption properties of the as-prepared samples were evaluated through UV−vis DRS technology. As shown in Figure 3B, the single-phase g-C_3N_4 and Bi_2O_3 had an optical absorption edge at approximately 480 and 450 nm, respectively; the result was similar to previous study.[4,29] Obviously, the single-phase Bi_2O_3 exhibited a strong absorptive capacity for UV (λ < 420 nm) but had no obvious response to visible light. However, the single-phase g-C_3N_4 was sensitive to both UV and visible light. Unlike the above two single-component photocatalysts, binary composite CB had the stronger ability to absorb visible light, which was due to the formation of a heterojunction between two components.[26] As for the CBH composite, when N-HMCs were introduced, redshift and enhanced visible absorbance were observed, and the optical absorption edge of CBH was about 500 nm. Moreover, the binary composite BH and CH also exhibited significant absorbance in the visible light region, which could be due to the dark color of N-HMCs sample, and the carbonate species could enhance visible-light absorption significantly, as proven by previous studies.[30,31,33,34] These results indicated that the doping of N-HMCs played a significant role in promoting the visible light adsorption of CBH composite; in other words, N-HMCs might be deemed as a photosensitizer which could be conducive to improve light absorption and electron transfer of the composite under visible-light irradiation, thus enhancing the photocatalytic activity.[30,50,51]

Generally, the band gap energy (E_g) of a semiconductor could be calculated according to Kubelka−Munk equation:[52] $\alpha\hbar\nu = A(h\nu - E_g)^{n/2}$, where α, $\hbar$, ν, and A represent the absorption coefficient, Planck constant, light frequency, and a constant, respectively.[4] In this study, n = 4 for indirect transition (g-C_3N_4), and n = 1 for direct transition (Bi_2O_3). The lower E_g would contribute to enhancing light absorption by the photocatalyst. Therefore, according to the calculation, the E_g values of BO and CN were 2.80 and 2.56, respectively (Figure 3C), similar to the previous studies.[4]

The transient photocurrent test was implemented to study the photocurrent responses and photoexcited charges recombination efficiency of the BO, CN, CB, and CBH. As shown in Figure 3D, the current density of CBH was about 118.76 nA $(cm^2)^{-1}$ under visible-light irradiation, and it was about 1.39, 1.90, and 8.78 times CB, CN, and BO, respectively. It was obvious that the CBH composite had the optimal photocurrent response under visible-light irradiation, which manifested the superior separation efficiency of photoexcited charges and more efficient electron migration at the interfaces.

DOI: 10.1021/acssuschemeng.8b03480
ACS Sustainable Chem. Eng. XXXX, XXX, XXX−XXX

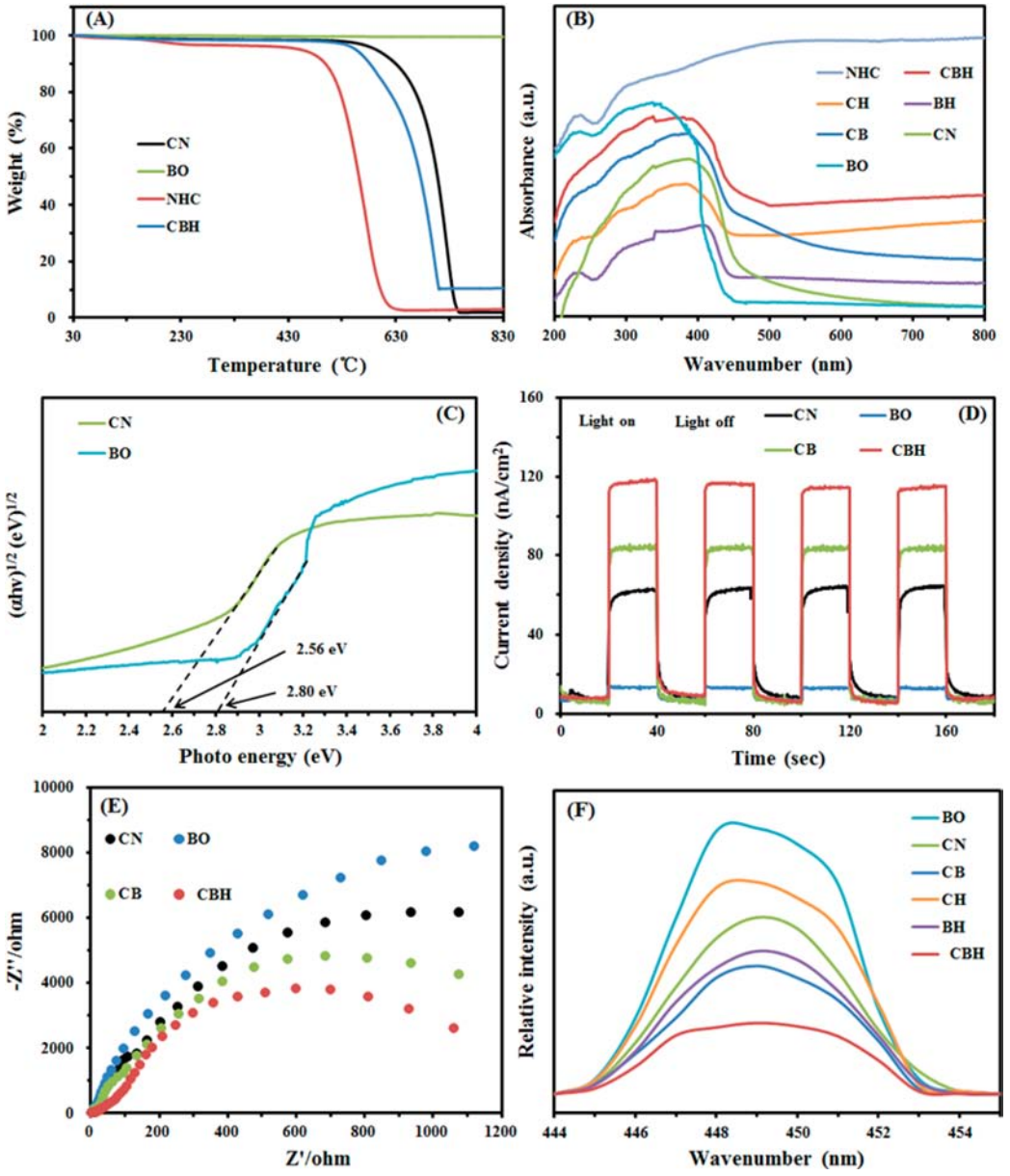

Figure 3. TGA curves of the as-prepared samples (A). UV−vis spectrum of the as-prepared samples (B). Band gap energies of g-C_3N_4 and Bi_2O_3 (C). Transient photocurrent of the as-prepared samples (D). EIS for different catalyst under visible-light irradiation (E). Photoluminescence spectra of the as-prepared samples (F).

Meanwhile, the arc radius in the electrochemical impedance spectra (EIS) Nyquist could be a credible way to estimate the charge transfer rate. It was widely believed that a smaller arc in the EIS Nyquist plot meant less charge migration resistance. As obviously displayed in Figure 3E, the CBH composite performed the lowest charge transfer resistance due to the smallest arc in the EIS Nyquist plot. The high transient photocurrent response and low charge transfer resistance of CBH composite could be caused by developing of the heterojunction between g-C_3N_4 and Bi_2O_3, and the N-HMCs could act as an efficient electronic conductor to accelerate photoexcited electron transfer and hinder the e^-−h^+ pairs recombination.

For understanding the migration and recombination process of photogenerated carries, the photoluminescence (PL) spectra was introduced. As shown in Figure 3F, all photocatalysts had strong emissions revolving around 444−454 nm on account of the recombination of e^-−h^+ pairs, and the CBH composite had lower PL emission intensity compared with those of other photocatalysts, which indicated the CBH composite had less recombination of e^-−h^+ pairs and better photocatalytic capability. These results may be caused by the excellent electrochemical performance of N-HMCs, and the synergistic effect between N-HMCs and CB heterojunction contributed to improving the charge separation efficiency, effectively reducing the recombination of e^-−h^+ pairs and prolonging charge carrier lifetime.[11,53]

Photocatalytic Efficiency and Photocatalyst Stability. The photocatalytic efficiency of the as-prepared photocatalysts was assessed through the photodegradation of two common antibiotics (namely, TCH and CFH) under visible-light irradiation. The photocatalytic activity of pure N-HMCs for TCH degradation also was investigated (Figure S8). The results demonstrated that the as-prepared photocatalysts had

DOI: 10.1021/acssuschemeng.8b03480
ACS Sustainable Chem. Eng. XXXX, XXX, XXX−XXX

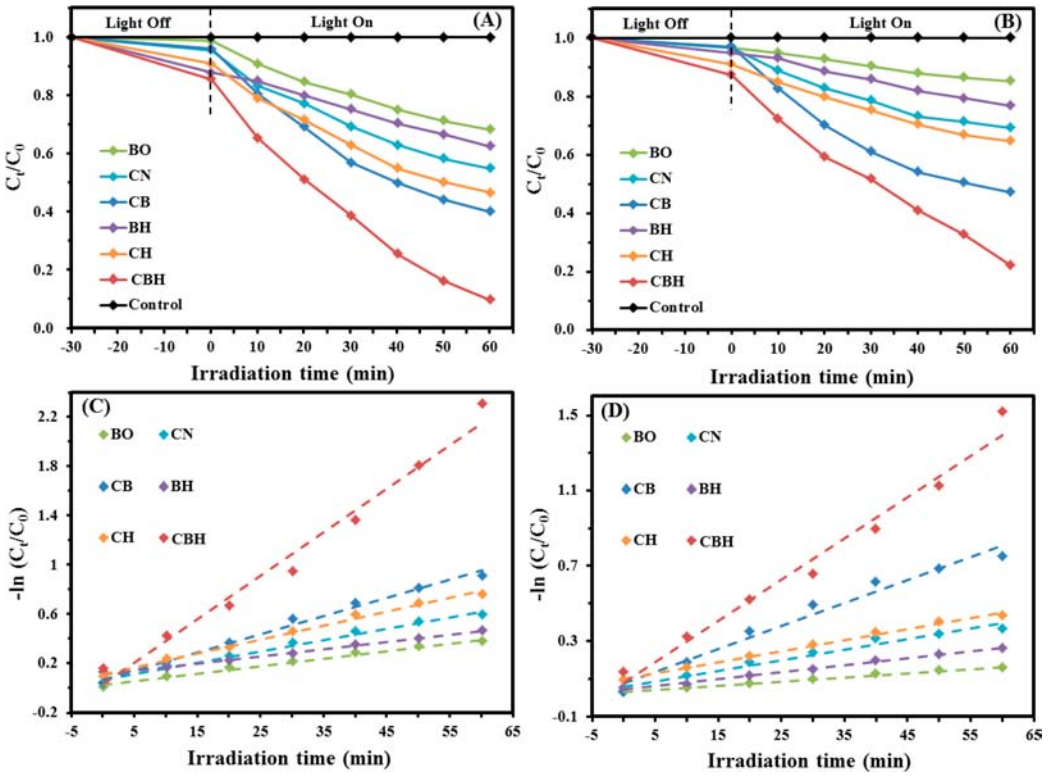

Figure 4. Photocatalytic activities of as-prepared samples for TCH (A) and CFH (B) degradation under visible-light (λ > 420 nm); pseudo-first-order kinetic models for the photodegradation of TCH (C) and CFH (D).

low adsorption capacity for both two antibiotics. However, compared to the samples of CN, BO, and CB, the N-HMCs-doped samples (namely, CH, BH, and CBH) showed superior adsorption performance; the results may be attributed to N-HMCs, which possessed high specific surface area and excellent pore structure. The adsorption removal efficiencies of TCH and CFH by CBH were 14.41 and 12.70%, respectively (Figure 4A,B). Some previous studies also indicated that the adsorption performance of photocatalyst could be improved after the doping of porous carbon.[34,54] As displayed in Figure 4A,B, the TCH and CFH were both stable under visible-light irradiation without a photocatalyst. However, the different photodegradation efficiency appearing under different photocatalysts and different antibiotics. Figure 4A showed that the CBH composite had the best photocatalytic efficiency for degrading TCH. Meanwhile, the photodegradation efficiency of the binary composites (BH, CH, and CB) were superior to the corresponding single-phase samples (g-C_3N_4 and Bi_2O_3), and they were in the order of CBH > CB > CH > CN > BH > BO. The single-phase Bi_2O_3 showed the lowest photodegradation efficiency of only 31.67% under visible-light irradiation for 1 h. However, the removal efficiency was 45.01% by single-phase g-C_3N_4. The reason might be that single-phase g-C_3N_4 had the better surface and structural characteristics, the higher visible-light absorption performance, and the slow e^-−h^+ recombination compared with that of single-phase Bi_2O_3. While the TCH removal efficiencies by binary composites of BH, CH, and CB were 37.35, 53.30, and 68.78%, respectively, the highest removal efficiency was 90.06% by ternary composite CBH. The increased photocatalytic efficiency by these composites could be due to the existence of heterojunction after the incorporation between the different materials, and the synergistic effects between each component could improve visible-light absorption, quicken the separation of e^-−h^+, and optimize the surface and structural characteristics, which confirmed by UV−vis spectrum, PL emission spectra, and N_2 adsorption−desorption isotherms, respectively. Figure 4B showed the photocatalytic efficiency of CFH. The degradation behavior was similar to that of the TCH, namely, the photodegradation efficiency was in the order of CBH > CB > CH > CN > BH > BO. Differently, the photocatalysts had lower degradation efficiency of CFH, and the maximum degradation efficiency only was 78.06%. The different degradation efficiencies of TCH and CFH in the photocatalytic system might be due to their different structures.[55] Furthermore, to identify the role of N doping, the photocatalytic performance of N-HMCs-modified g-C_3N_4/Bi_2O_3 and HMCs-modified g-C_3N_4/Bi_2O_3 were investigated. As displayed in Figure S9, it is obvious that the N-HMCs modified g-C_3N_4/Bi_2O_3 possesses better photocatalytic performance, which might be because the N doping improved the physicochemical properties of HMCs and increased charge carrier transfer in HMCs.[35,56]

To deepen the understanding of the photocatalytic process, the pseudo-first-order kinetic model was introduced to evaluate the experimental results. The kinetic model was expressed as follows: $-\ln(C_t/C_0) = kt$, where C_t, C_0, k, and t represent the instant antibiotic concentration, initial antibiotic concentration, rate constant, and reaction time, respectively. Analysis for linear fitting results displayed in Figure 4C,D, and the corresponding parameters listed in Table S2. It was obvious that the photocatalytic process fitted well with the pseudo-first-order model (R^2 > 0.97). Considering the rate constant (Table S2), k for TCH degradation over CBH composite (0.0354 min^{-1}) was approximately 2.39, 3.13, 3.85,

DOI: 10.1021/acssuschemeng.8b03480
ACS Sustainable Chem. Eng. XXXX, XXX, XXX−XXX

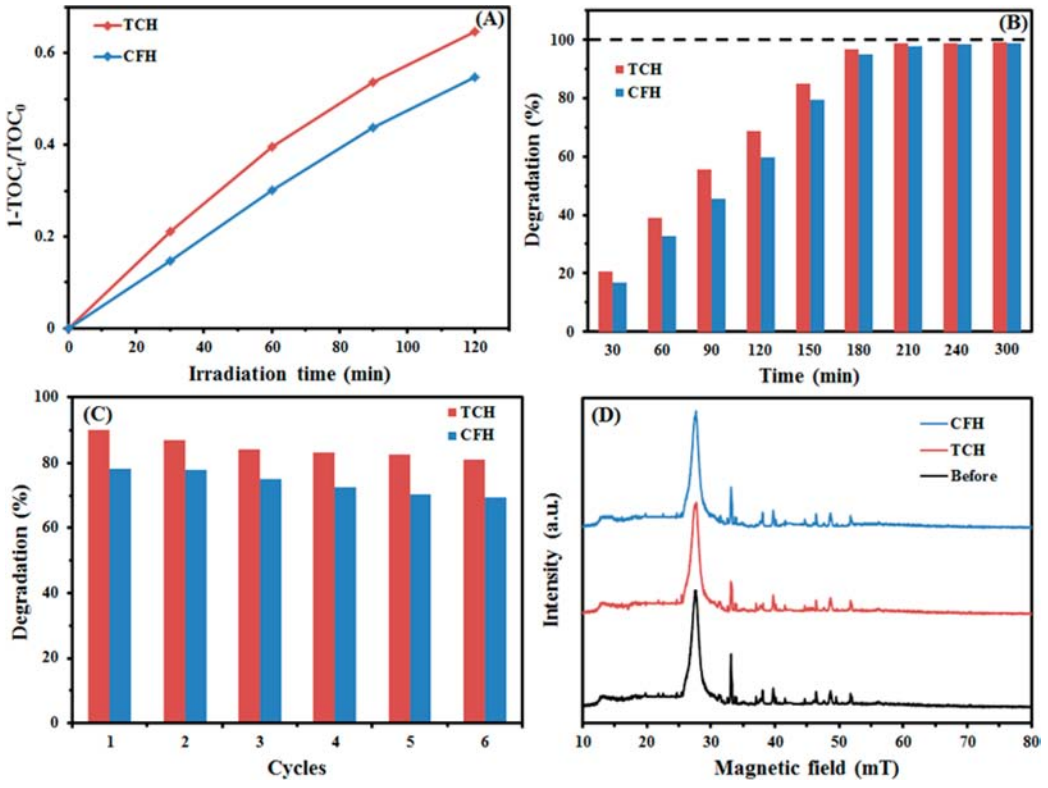

Figure 5. TOC removal of TCH and CFH by CBH composite irradiation for 120 min (A) and 300 min (B); cyclic photocatalytic experiments of CBH photocatalyst for degradation of antibiotics (C). XRD pattern of the CBH sample after six cycles of photocatalytic experiments (D).

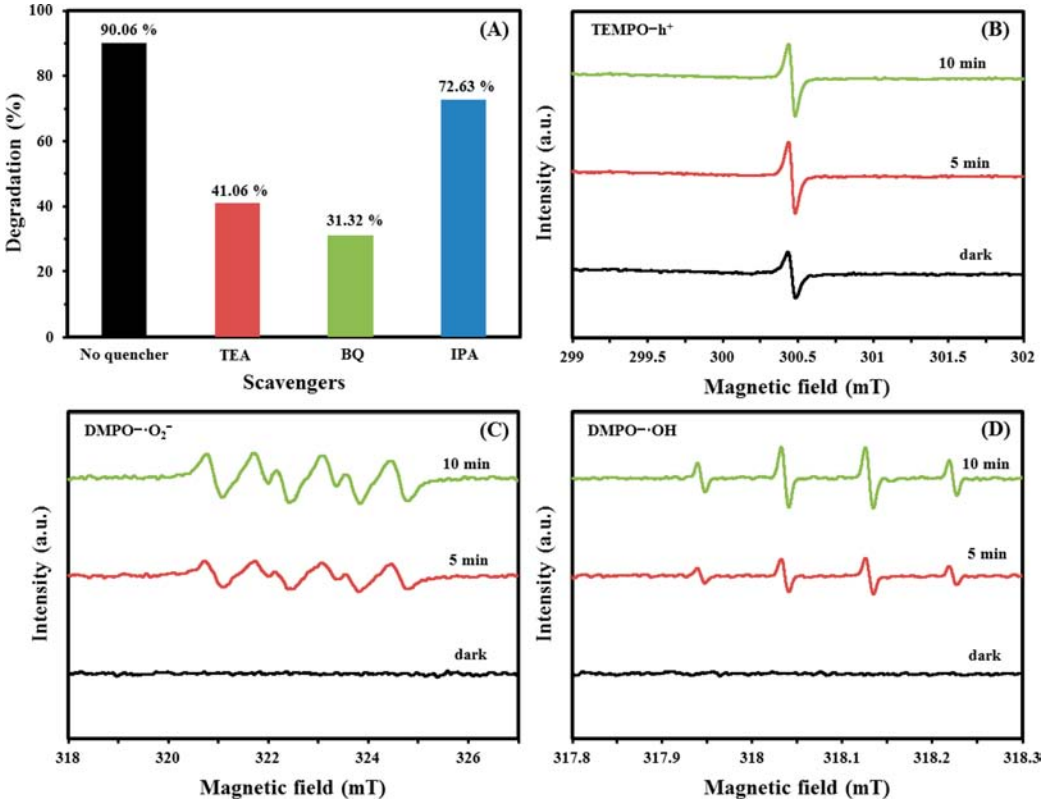

Figure 6. Trapping experiment of active species during the photocatalytic degradation of TCH over CBH composite under visible-light irradiation (A). ESR spectra of radical adducts trapped by TEMPO (h^+) and DMPO ($^{\bullet}O_2^-$ and $^{\bullet}$OH) in CBH dispersion in the dark and under visible-light irradiation: in aqueous dispersion for TEMPO−h^+ (B); in methanol dispersion for DMPO−$^{\bullet}O_2^-$ (C); in aqueous dispersion for DMPO−$^{\bullet}$OH (D).

DOI: 10.1021/acssuschemeng.8b03480
ACS Sustainable Chem. Eng. XXXX, XXX, XXX−XXX

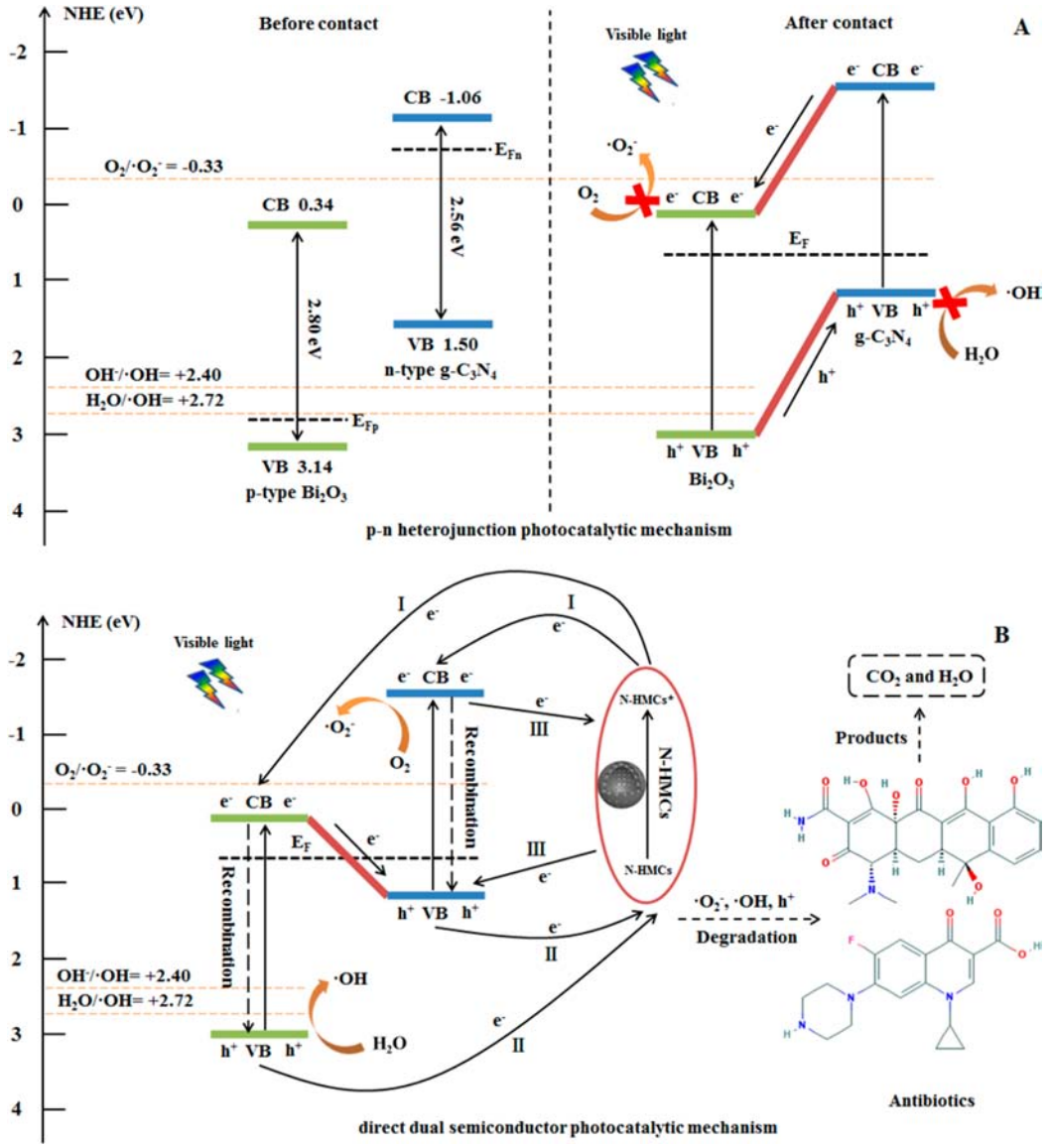

Figure 7. Schematic diagram for possible charge separation and photocatalytic mechanism of CBH composite.

6.10, and 5.80 times superior to those of CB (0.0148 min^{-1}), CH (0.0113 min^{-1}), CN (0.0092 min^{-1}), BH (0.0058 min^{-1}), and BO (0.0061 min^{-1}), respectively. Meanwhile, k values for CFH degradation over CBH, CB, CH, CN, BH, and BO were 0.0218, 0.0122, 0.0062, 0.0058, 0.0037, and 0.0022 min^{-1}, respectively. According to the values of k, the CBH composite displayed the highest photodegradation rate for both TCH and CFH, and the photodegradation rate of TCH was faster than that of CFH. These simulated results were consistent with the experimental results. These results demonstrated that the preparation of CBH composite could significantly enhance the photocatalytic activity of single-phase g-C_3N_4 or Bi_2O_3.

For evaluating the mineralization efficiency of antibiotic by CBH composite, the total organic carbon (TOC) analysis was adopted. Figure 5A showed that the mineralization efficiency of TCH was higher than that of CFH, 64.70 and 54.80%, respectively, within the irradiation of 2 h. However, after irradiation for 3.5 h, the TOC was almost eliminated for both antibiotics (Figure 5B).

Stability is an important parameter of the photocatalyst, which is significant to evaluate the practical application of photocatalyst. To investigate the stability of CBH composite, the TCH and CFH photocatalytic experiments of the CBH composite were performed for six cycles. After each repetition, the CBH composite was recycled through centrifugation, washing, and drying for the next cycle. As shown in Figure 5C, the photocatalytic efficiency of CBH composite was down only 9.03 and 8.67% for the degradation of TCH and CFH, respectively, after six cyclic experiments under visible-light irradiation. Meanwhile, the XRD image (Figure 5D) manifested that the crystal structure of the CBH composite had almost no significant change before and after the cyclic experiments. The results manifested that the CBH composite showed magnificent stability and had great promise in practical application.

Photocatalytic Mechanism. The CBH composite showed wonderful photocatalytic degradation efficiency of two antibiotics, and the abundant active substances should be responsible for strong redox capacity.[12] For exploring the major active substances involved in the TCH photodegradation process, scavenger experiments were performed. Three typical chemicals, namely, triethanolamine (TEA), *p*-

DOI: 10.1021/acssuschemeng.8b03480
ACS Sustainable Chem. Eng. XXXX, XXX, XXX−XXX

benzoquinone (BQ), and isopropanol (IPA), were employed as the scavengers of the hole (h^+), superoxide radical ($^\bullet O_2^-$), and hydroxyl radical ($^\bullet OH$), respectively. As shown in Figure 6A, when 1 mM scavengers was injected into the photocatalytic system, the photodegradation efficiency of TCH was obviously suppressed. The degradation efficiency of TCH decreased to 41.06, 31.32, and 72.63% in the presence of TEA, BQ, and IPA, respectively. These results revealed that the h^+, $^\bullet O_2^-$, and $^\bullet OH$ had great significance in the photodegradation of TCH, and the ranking of impact was $^\bullet O_2^- > h^+ > {}^\bullet OH$.

For further validating the existence of these active substances in the photocatalytic process under visible irradiation, the ESR spin-trap with DMPO and TEMPO techniques were introduced. All the tests were implemented under the dark condition and visible-light irradiation of 5 and 10 min. According to the Figure 6B, there was an obvious peak in the dark condition for TEMPO−h^+. However, the characteristic peak of TEMPO−h^+ became stronger after the photocatalyst was presented to visible light, which suggested that the hole played a significant role in the photodegradation process. As depicted in Figure 6C,D, there were obviously no peaks under the dark conditions for both DMPO−$^\bullet O_2^-$ and DMPO−$^\bullet OH$. However, after the photocatalysts were presented to visible light, the characteristic peaks of both DMPO−$^\bullet O_2^-$ and DMPO−$^\bullet OH$ were intense, and the signal strength increased with the irradiation time. These results proved that the $^\bullet O_2^-$ and $^\bullet OH$ presented in CBH photodegradation system. The scavenger experiments and ESR results both confirmed that the h^+, $^\bullet O_2^-$, and $^\bullet OH$ acted together on the photodegradation of TCH by CBH composite.

According to the above experimental results, a plausible mechanism of photodegradation of antibiotics by CBH composite was proposed. The VB and CB edge positions of the CBH composite can be calculated according to the following formula: $E_{CB} = X - E^e - 1/2E_g$, $E_{VB} = E_{CB} + E_g$, where X represents the electronegativity of the semiconductor, and the values of X are about 4.72 and 6.24 eV for g-C_3N_4 and Bi_2O_3, respectively. E^e is the energy of free electrons on the hydrogen scale (approximately 4.5 eV). It is calculated that E_{CB} is −1.06 and 0.34 eV for g-C_3N_4 and Bi_2O_3, respectively, and E_{VB} is 1.5 and 3.14 eV, respectively. These results are similar to those of previous studies.[4]

It is well-known that the oxidizability and reducibility of the semiconductor photocatalyst depend on the potential of VB and CB, respectively.[26] When combined with Bi_2O_3 and g-C_3N_4, the heterojunction photocatalyst CB would be formed, and the possible charge separation pathways of photoexcited e^-−h^+ might be described as follows: First, when forming a heterojunction, two possible charge separation pathways may be present between g-C_3N_4 and Bi_2O_3 (namely, p−n heterojunction photocatalytic system and direct dual semiconductor photocatalytic system). As depicted in Figure 7A, before contact, the Fermi level (dotted line) is the chemical potential of thermodynamic equilibrium, the Fermi levels of p-type Bi_2O_3 (E_{Fp}) and n-type g-C_3N_4 (E_{Fn}) semiconductors was approximately close to VB and CB, respectively.[57] However, after contact to form a heterojunction, the Fermi levels of g-C_3N_4 and Bi_2O_3 will achieve equilibrium (E_F). Simultaneously, the VB edge of Bi_2O_3 and g-C_3N_4 would rise to 0.19 and −1.45 eV, respectively, under visible light with energy less than 2.95 eV (λ > 420 nm).[58,59] When the CBH composite was exposed to visible light, the photoexcited electrons would transfer from VB into CB of Bi_2O_3 remaining holes in the VB. Meanwhile, the same procedure happened in g-C_3N_4. If following the p−n heterojunction photocatalytic mechanism, then the electrons in the CB of the g-C_3N_4 would transfer to the CB of Bi_2O_3, and the holes transferred in the opposite direction. The electrons and holes would accumulate in Bi_2O_3 CB and g-C_3N_4 VB, respectively.[57,60,61] If correct, then the accumulated electrons on the CB of Bi_2O_3 could not reduce O_2 to generate $^\bullet O_2^-$ due to the CB of Bi_2O_3 being more positive than the potential of $O_2/^\bullet O_2^-$ (−0.33 eV).[26] Additionally, the holes of g-C_3N_4 could not oxidize OH^- or H_2O to form $^\bullet OH$ because of the VB potential of g-C_3N_4 was below standard redox potential of $OH^-/^\bullet OH$ (2.40 eV) and $H_2O/^\bullet OH$ (2.72 eV) (Figure 7A).[4] However, the above experimental results revealed that h^+, $^\bullet O_2^-$, and $^\bullet OH$ were the dominating active substances in the CBH photocatalytic system, which indicated the separation process of the photoexcited e^-−h^+ pairs could not follow the p−n heterojunction photocatalytic mechanism. The second pathway was the direct dual semiconductor photocatalytic system (Figure 7B), namely, the electrons in the CB of Bi_2O_3 could transfer to the VB of g-C_3N_4. After that, the accumulated electrons in g-C_3N_4 CB had more negative potential to reduce O_2 to generate $^\bullet O_2^-$, and the holes remaining in Bi_2O_3 VB had more positive potential oxidize H_2O or pollutant to form $^\bullet OH$.[62] Therefore, it confirmed that the g-C_3N_4/Bi_2O_3 heterojunction follows the direct dual semiconductor photocatalytic mechanism. Meanwhile, the introduction of N-HMCs also played a significant effect on the activity of CBH and can be explained as follows (Figure 7B): (1) According to the UV−vis spectrum results, the N-HMCs could serve as a photosensitizer; thus, N-HMCs could absorb the irradiation and infuse the photoexcited electrons into the CB of g-C_3N_4 or Bi_2O_3 (step I).[30,33,34] (2) The electrons from the VB of g-C_3N_4 or Bi_2O_3 could be transferred to the positively charged N-HMCs and leave the holes (step II).[30,33] Meanwhile, the photoexcited charge carrier is easy to recombine and emit energy; the N-HMCs could be an electron tunnel enabling the electrons to leave the surface of g-C_3N_4 or Bi_2O_3, thus decreasing the recombination of e^-−h^+ pairs and extending charge carrier life, which can be proved by the lower charge transfer resistance and lower PL motion (step III).[31,32,63] Additionally, the N_2 sorption analysis results indicated N-HMCs doping could modify the surface properties of the CBH composite,[33,63] which can significantly improve the contact between pollutants and photocatalyst and enhance the photocatalytic efficiency. In a word, the excellent photocatalytic efficiency of CBH composite attributed to the synergistic action of g-C_3N_4/Bi_2O_3 direct dual semiconductor photocatalytic system and the N-HMCs, and the N-HMCs play a significant role in improving the photocatalytic performance of the g-C_3N_4/Bi_2O_3@N-HMCs photocatalytic system.

CONCLUSIONS

In conclusion, the novel visible-light photocatalyst of CBH composite was successfully prepared by a facile thermal process. The prepared CBH composite showed better photodegradation efficiency of antibiotics (i.e., TCH and CFH) than did single-phase g-C_3N_4, Bi_2O_3 and binary composites under the visible-light irradiation. Various characterization techniques indicated that the increased photocatalytic efficiency of CBH composite was attributed to the synergistic action of g-C_3N_4/Bi_2O_3 direct dual semiconductor

DOI: 10.1021/acssuschemeng.8b03480
ACS Sustainable Chem. Eng. XXXX, XXX, XXX−XXX

photocatalytic system and the N-HMCs. Significantly, N-HMCs play vital roles in improving visible-light absorption, accelerating electron transfer, hindering the electron−hole pairs recombination, and provided more active sites in the photocatalytic process. The scavenger experiments and ESR dates revealed that active substances h^+, $^\bullet O_2^-$, and $^\bullet OH$ performed together in the photodegradation system. Additionally, the CBH composite performed superior photostability after six rounds of recycling, which is significant to the practical application of photocatalyst. The current study might inspire some new ideas for constructing novel and efficient heterostructure photocatalysts and facilitated their practical application in environmental remediation.

■ ASSOCIATED CONTENT

Supporting Information

The Supporting Information is available free of charge on the ACS Publications website at DOI: 10.1021/acssuschemeng.8b03480.

Details of N-HMCs synthesis; figures of the EDS pattern, XRD pattern, XPS spectrum, element mapping, N_2 adsorption−desorption isotherms, and the photocatalytic activity of as-prepared samples; tables of the element content in samples and the results of the pseudo-first-order model (PDF)

■ AUTHOR INFORMATION

Corresponding Authors

*E-mail: zhifengliu@hnu.edu.cn. Tel.: 86-731-88821697 (Z.L.).

*E-mail: zgming@hnu.edu.cn. Tel.: 86-731-8-8823701 (G.Z.).

ORCID

Zhifeng Liu: 0000-0002-8598-4656

Guangming Zeng: 0000-0002-4230-7647

Author Contributions

B.S. and Z.L. contributed equally to this article.

Notes

The authors declare no competing financial interest.

■ ACKNOWLEDGMENTS

The study was financially supported by the Program for Changjiang Scholars and Innovative Research Team in University (IRT-13R17), the National Natural Science Foundation of China (51679085, 51378192, 51378190, 51521006, 51508177), and the Fundamental Research Funds for the Central Universities of China (No. 531107050930).

■ REFERENCES

(1) Zhang, C.; Lai, C.; Zeng, G.; Huang, D.; Yang, C.; Wang, Y.; Zhou, Y.; Cheng, M. Efficacy of carbonaceous nanocomposites for sorbing ionizable antibiotic sulfamethazine from aqueous solution. *Water Res.* **2016**, *95*, 103−112.

(2) Liu, Y.; Zeng, G.; Zhong, H.; Wang, Z.; Liu, Z.; Cheng, M.; Liu, G.; Yang, X.; Liu, S. Effect of rhamnolipid solubilization on hexadecane bioavailability: enhancement or reduction? *J. Hazard. Mater.* **2017**, *322*, 394−401.

(3) Shao, B.; Liu, Z.; Zeng, G.; Liu, Y.; Yang, X.; Zhou, C.; Chen, M.; Liu, Y.; Jiang, Y.; Yan, M. Immobilization of laccase on hollow mesoporous carbon nanospheres: Noteworthy immobilization, excellent stability and efficacious for antibiotic contaminants removal. *J. Hazard. Mater.* **2019**, *362*, 318−326.

(4) Jiang, L.; Yuan, X.; Zeng, G.; Liang, J.; Chen, X.; Yu, H.; Wang, H.; Wu, Z.; Zhang, J.; Xiong, T. In-situ synthesis of direct solid-state dual Z-scheme WO3/g-C3N4/Bi2O3 photocatalyst for the degradation of refractory pollutant. *Appl. Catal., B* **2018**, *227*, 376−385.

(5) Shao, B.; Liu, Z.; Zhong, H.; Zeng, G.; Liu, G.; Yu, M.; Liu, Y.; Yang, X.; Li, Z.; Fang, Z.; et al. Effects of rhamnolipids on microorganism characteristics and applications in composting: A review. *Microbiol. Res.* **2017**, *200*, 33−44.

(6) Chen, M.; Xu, P.; Zeng, G.; Yang, C.; Huang, D.; Zhang, J. Bioremediation of soils contaminated with polycyclic aromatic hydrocarbons, petroleum, pesticides, chlorophenols and heavy metals by composting: Applications, microbes and future research needs. *Biotechnol. Adv.* **2015**, *33*, 745−755.

(7) Liu, Z.; Shao, B.; Zeng, G.; Chen, M.; Li, Z.; Liu, Y.; Jiang, Y.; Zhong, H.; Liu, Y.; Yan, M. Effects of rhamnolipids on the removal of 2,4,2,4-tetrabrominated biphenyl ether (BDE-47) by Phanerochaete chrysosporium analyzed with a combined approach of experiments and molecular docking. *Chemosphere* **2018**, *210*, 922−930.

(8) Liang, C.; Niu, C.-G.; Zhang, L.; Wen, X.-J.; Yang, S.-F.; Guo, H.; Zeng, G.-M. Construction of 2D heterojunction system with enhanced photocatalytic performance: Plasmonic Bi and reduced graphene oxide co-modified Bi5O7I with high-speed charge transfer channels. *J. Hazard. Mater.* **2019**, *361*, 245−258.

(9) Shan, W.; Hu, Y.; Bai, Z.; Zheng, M.; Wei, C. In situ preparation of g-C3N4/bismuth-based oxide nanocomposites with enhanced photocatalytic activity. *Appl. Catal., B* **2016**, *188*, 1−12.

(10) Fujishima, A.; Honda, K. Electrochemical Photolysis of Water at a Semiconductor Electrode. *Nature* **1972**, *238*, 37.

(11) Ng, Y. H.; Ikeda, S.; Matsumura, M.; Amal, R. A perspective on fabricating carbon-based nanomaterials by photocatalysis and their applications. *Energy Environ. Sci.* **2012**, *5* (11), 9307−9318.

(12) Zhu, Z.; Murugananthan, M.; Gu, J.; Zhang, Y. Fabrication of a Z-Scheme g-C3N4/Fe-TiO2 Photocatalytic Composite with Enhanced Photocatalytic Activity under Visible Light Irradiation. *Catalysts* **2018**, *8* (3), 112.

(13) Fu, J.; Yu, J.; Jiang, C.; Cheng, B. g-C3N4-Based Heterostructured Photocatalysts. *Adv. Energy Mater.* **2018**, *8*, 1701503.

(14) Liang, C.; Niu, C. G.; Guo, H.; Huang, D.; Wen, X. J.; Yang, S. F.; Zeng, G. Combination of efficient charge-separation process with the assistance of novel dual Z-scheme system: self-assembly photocatalyst of Ag@AgI/BiOI modified oxygen-doped carbon nitride nanosheet with enhanced photocatalytic performance. *Catal. Sci. Technol.* **2018**, *8*, 1161.

(15) Jiang, L.; Yuan, X.; Zeng, G.; Chen, X.; Wu, Z.; Liang, J.; Zhang, J.; Wang, H.; Wang, H. Phosphorus- and Sulfur-Codoped g-C3N4: Facile Preparation, Mechanism Insight, and Application as Efficient Photocatalyst for Tetracycline and Methyl Orange Degradation under Visible Light Irradiation. *ACS Sustainable Chem. Eng.* **2017**, *5* (7), 5831−5841.

(16) Yang, X.; Qian, F.; Zou, G.; Li, M.; Lu, J.; Li, Y.; Bao, M. Facile fabrication of acidified g-C3N4/g-C3N4 hybrids with enhanced photocatalysis performance under visible light irradiation. *Appl. Catal., B* **2016**, *193*, 22−35.

(17) Liang, J.; Zheng, Y.; Chen, J.; Liu, J.; Hulicova-Jurcakova, D.; Jaroniec, M.; Qiao, S. Z. Facile Oxygen Reduction on a Three-Dimensionally Ordered Macroporous Graphitic C3N4/Carbon Composite Electrocatalyst. *Angew. Chem., Int. Ed.* **2012**, *51* (16), 3892−3896.

(18) Li, H.; Tu, W.; Zhou, Y.; Zou, Z. Z-Scheme Photocatalytic Systems for Promoting Photocatalytic Performance: Recent Progress and Future Challenges. *Adv. Sci.* **2016**, *3* (11), 1500389.

(19) Ohtani, B. Photocatalysis A to Z—What we know and what we do not know in a scientific sense. *J. Photochem. Photobiol., C* **2010**, *11* (4), 157−178.

(20) Natarajan, T. S.; Thampi, K. R.; Tayade, R. J. Visible Light Driven Redox-mediator-free Dual Semiconductor Photocatalytic Systems for Pollutant Degradation and the Ambiguity in Applying Z-scheme Concept. *Appl. Catal., B* **2018**, *227*, 296−311.

DOI: 10.1021/acssuschemeng.8b03480
ACS Sustainable Chem. Eng. XXXX, XXX, XXX−XXX

(21) He, Y.; Zhang, L.; Teng, B.; Fan, M. New application of Z-scheme Ag3PO4/g-C3N4 composite in converting CO2 to fuel. *Environ. Sci. Technol.* **2015**, *49* (1), 649−656.
(22) Hong, Y.; Jiang, Y.; Li, C.; Fan, W.; Yan, X.; Yan, M.; Shi, W. In-situ synthesis of direct solid-state Z-scheme V2O5/g-C3N4 heterojunctions with enhanced visible light efficiency in photocatalytic degradation of pollutants. *Appl. Catal., B* **2016**, *180*, 663−673.
(23) Ye, R.; Fang, H.; Zheng, Y. Z.; Li, N.; Wang, Y.; Tao, X. Fabrication of CoTiO3/g-C3N4 Hybrid Photocatalysts with Enhanced H2 Evolution: Z-Scheme Photocatalytic Mechanism Insight. *ACS Appl. Mater. Interfaces* **2016**, *8* (22), 13879−13889.
(24) Wang, J.; Yao, H. C.; Fan, Z. Y.; Zhang, L.; Wang, J.; Zang, S. Q.; Li, Z. Indirect Z-scheme BiOI/g-C3N4 Photocatalysts with Enhanced Photoreduction CO2 Activity under Visible Light Irradiation. *ACS Appl. Mater. Interfaces* **2016**, *8* (6), 3765−3775.
(25) Lv, J.; Dai, K.; Zhang, J.; Geng, L.; Liang, C.; Liu, Q.; Zhu, G.; Chen, C. Facile synthesis of Z-scheme graphitic-C3N4/Bi2MoO6 nanocomposite for enhanced visible photocatalytic properties. *Appl. Surf. Sci.* **2015**, *358*, 377−384.
(26) Zhang, J.; Hu, Y.; Jiang, X.; Chen, S.; Meng, S.; Fu, X. Design of a direct Z-scheme photocatalyst: preparation and characterization of Bi2O3/g-C3N4 with high visible light activity. *J. Hazard. Mater.* **2014**, *280*, 713−722.
(27) Wang, J.; Tang, L.; Zeng, G.; Liu, Y.; Zhou, Y.; Deng, Y.; Wang, J.; Peng, B. Plasmonic Bi Metal Deposition and g-C3N4 Coating on Bi2WO6Microspheres for Efficient Visible-Light Photocatalysis. *ACS Sustainable Chem. Eng.* **2017**, *5* (1), 1062−1072.
(28) He, R.; Zhou, J.; Fu, H.; Zhang, S.; Jiang, C. Room-temperature in situ fabrication of Bi2O3/g-C3N4 direct Z-scheme photocatalyst with enhanced photocatalytic activity. *Appl. Surf. Sci.* **2018**, *430*, 273−282.
(29) Zhang, L.; Wang, G.; Xiong, Z.; Tang, H.; Jiang, C. Fabrication of flower-like direct Z-scheme β-Bi2O3/g-C3N4 photocatalyst with enhanced visible light photoactivity for Rhodamine B degradation. *Appl. Surf. Sci.* **2018**, *436*, 162−171.
(30) Zhao, W.; Wang, Y.; Yang, Y.; Tang, J.; Yang, Y. Carbon spheres supported visible-light-driven CuO-BiVO 4 heterojunction: Preparation, characterization, and photocatalytic properties. *Appl. Catal., B* **2012**, *115−116* (5), 90−99.
(31) Liu, S.; Ke, J.; Sun, H.; Liu, J.; Tade, M. O.; Wang, S. Size dependence of uniformed carbon spheres in promoting graphitic carbon nitride toward enhanced photocatalysis. *Appl. Catal., B* **2017**, *204*, 358−364.
(32) Zhao, X.; Su, S.; Wu, G.; Li, C.; Qin, Z.; Lou, X.; Zhou, J. Facile synthesis of the flower-like ternary heterostructure of Ag/ZnO encapsulating carbon spheres with enhanced photocatalytic performance. *Appl. Surf. Sci.* **2017**, *406*, 254−264.
(33) Wu, J.; Chen, X.; Li, C.; Qi, Y.; Qi, X.; Ren, J.; Yuan, B.; Ni, B.; Zhou, R.; Zhang, J.; et al. Hydrothermal synthesis of carbon spheres − BiOI/BiOIO3 heterojunctions for photocatalytic removal of gaseous Hg 0 under visible light. *Chem. Eng. J.* **2016**, *304*, 533−543.
(34) Gamage McEvoy, J.; Cui, W.; Zhang, Z. Synthesis and characterization of Ag/AgCl−activated carbon composites for enhanced visible light photocatalysis. *Appl. Catal., B* **2014**, *144* (2), 702−712.
(35) Zhou, T.; Zhou, Y.; Ma, R.; Zhou, Z.; Liu, G.; Liu, Q.; Zhu, Y.; Wang, J. Nitrogen-doped hollow mesoporous carbon spheres as a highly active and stable metal-free electrocatalyst for oxygen reduction. *Carbon* **2017**, *114*, 177−186.
(36) Tang, J.; Liu, J.; Li, C.; Li, Y.; Tade, M. O.; Dai, S.; Yamauchi, Y. Synthesis of nitrogen-doped mesoporous carbon spheres with extra-large pores through assembly of diblock copolymer micelles. *Angew. Chem., Int. Ed.* **2014**, *54* (2), 588−593.
(37) Prieto, G.; Tüysüz, H.; Duyckaerts, N.; Knossalla, J.; Wang, G. H.; Schüth, F. Hollow Nano- and Microstructures as Catalysts. *Chem. Rev.* **2016**, *116* (22), 14056−14119.
(38) Feng, H. P.; Tang, L.; Zeng, G.; Tang, J.; Deng, Y.; Yan, M.; Liu, Y.; Zhou, Y.; Ren, X.; Chen, S. Carbon-based Core-shell Nanostructured Materials for Electrochemical Energy Storage. *J. Mater. Chem. A* **2018**, *6* (17), 7310−7337.
(39) Liu, Y.; Liu, Z.; Zeng, G.; Chen, M.; Jiang, Y.; Shao, B.; Li, Z.; Liu, Y. Effect of surfactants on the interaction of phenol with laccase: Molecular docking and molecular dynamics simulation studies. *J. Hazard. Mater.* **2018**, *357*, 10−18.
(40) Zhang, H.; Noonan, O.; Huang, X.; Yang, Y.; Xu, C.; Zhou, L.; Yu, C. Surfactant-Free Assembly of Mesoporous Carbon Hollow Spheres with Large Tunable Pore Sizes. *ACS Nano* **2016**, *10* (4), 4579−4586.
(41) Irmawati, R.; Noorfarizan Nasriah, M. N.; Taufiq-Yap, Y. H.; Abdul Hamid, S. B. Characterization of bismuth oxide catalysts prepared from bismuth trinitrate pentahydrate: influence of bismuth concentration. *Catal. Today* **2004**, *93-95* (1), 701−709.
(42) Chen, X.; Kierzek, K.; Jiang, Z.; Chen, H.; Tang, T.; Wojtoniszak, M.; Kalenczuk, R. J.; Chu, P. K.; Borowiakpalen, E. Synthesis, Growth Mechanism, and Electrochemical Properties of Hollow Mesoporous Carbon Spheres with Controlled Diameter. *J. Phys. Chem. C* **2011**, *115* (36), 17717−17724.
(43) Zhou, C.; Lai, C.; Huang, D.; Zeng, G.; Zhang, C.; Cheng, M.; Hu, L.; Wan, J.; Xiong, W.; Wen, M.; et al. Highly porous carbon nitride by supramolecular preassembly of monomers for photocatalytic removal of sulfamethazine under visible light driven. *Appl. Catal., B* **2018**, *220*, 202−210.
(44) Chen, W.; Liu, T. Y.; Huang, T.; Liu, X. H.; Yang, X. J. Novel mesoporous P-doped graphitic carbon nitride nanosheets coupled with ZnIn2S4 nanosheets as efficient visible light driven heterostructures with remarkably enhanced photo-reduction activity. *Nanoscale* **2016**, *8* (6), 3711.
(45) Chen, F.; Yang, Q.; Li, X.; Zeng, G.; Wang, D.; Niu, C.; Zhao, J.; An, H.; Xie, T.; Deng, Y. Hierarchical assembly of graphene-bridged Ag3PO4/Ag/BiVO4 (040) Z-scheme photocatalyst: An efficient, sustainable and heterogeneous catalyst with enhanced visible-light photoactivity towards tetracycline degradation under visible light irradiation. *Appl. Catal., B* **2017**, *200*, 330−342.
(46) Bai, X.; Wang, L.; Wang, Y.; Yao, W.; Zhu, Y. Enhanced oxidation ability of g-C3N4 photocatalyst via C 60 modification. *Appl. Catal., B* **2014**, *152−153* (1), 262−270.
(47) Liu, S.; Chen, J.; Xu, D.; Zhang, X.; Shen, M. Enhanced photocatalytic activity of direct Z-scheme Bi2O3/g-C3N4 composites via facile one-step fabrication. *J. Mater. Res.* **2018**, *33*, 1391−1400.
(48) Balachandran, S.; Swaminathan, M. Facile Fabrication of Heterostructured Bi2O3−ZnO Photocatalyst and Its Enhanced Photocatalytic Activity. *J. Phys. Chem. C* **2012**, *116* (50), 26306−26312.
(49) Chen, F.; Yang, Q.; Wang, Y.; Zhao, J.; Wang, D.; Li, X.; Guo, Z.; Wang, H.; Deng, Y.; Niu, C.; et al. Novel ternary heterojunction photcocatalyst of Ag nanoparticles and g-C3N4 nanosheets co-modified BiVO4 for wider spectrum visible-light photocatalytic degradation of refractory pollutant. *Appl. Catal., B* **2017**, *205*, 133−147.
(50) Yang, X.; Cao, C.; Hohn, K.; Erickson, L.; Maghirang, R.; Hamal, D.; Klabunde, K. Highly visible-light active C- and V-doped TiO 2 for degradation of acetaldehyde. *J. Catal.* **2007**, *252* (2), 296−302.
(51) Lettmann, C.; Hildenbrand, K.; Kisch, H.; Macyk, W.; Maier, W. F. Visible light photodegradation of 4-chlorophenol with a coke-containing titanium dioxide photocatalyst. *Appl. Catal., B* **2001**, *32* (4), 215−227.
(52) Xin, X.; Lang, J.; Wang, T.; Su, Y.; Zhao, Y.; Wang, X. Construction of novel ternary component photocatalyst Sr0.25H1.5Ta2O6·H2O coupled with g-C3N4 and Ag toward efficient visible light photocatalytic activity for environmental remediation. *Appl. Catal., B* **2016**, *181*, 197−209.
(53) Jo, W. K.; Selvam, N. C. S. Z-scheme CdS/g-C3N4 composites with RGO as an electron mediator for efficient photocatalytic H 2 production and pollutant degradation. *Chem. Eng. J.* **2017**, *317*, 913−924.

DOI: 10.1021/acssuschemeng.8b03480
ACS Sustainable Chem. Eng. XXXX, XXX, XXX−XXX

(54) Wang, Y.; Cai, Q.; Yao, M.; Kang, S.; Ge, Z.; Li, X. Easy Synthesis of Ordered Mesoporous Carbon−Carbon Nanotube Nanocomposite as a Promising Support for CO2 Photoreduction. *ACS Sustainable Chem. Eng.* **2018**, *6* (2), 2529−2534.
(55) Ding, H.; Wu, Y.; Zou, B.; Lou, Q.; Zhang, W.; Zhong, J.; Lu, L.; Dai, G. Simultaneous removal and degradation characteristics of sulfonamide, tetracycline, and quinolone antibiotics by laccase-mediated oxidation coupled with soil adsorption. *J. Hazard. Mater.* **2016**, *307*, 350−358.
(56) Han, J.; Xu, G.; Ding, B.; Pan, J.; Dou, H.; Macfarlane, D. Porous nitrogen-doped hollow carbon spheres derived from polyaniline for high performance supercapacitors. *J. Mater. Chem. A* **2014**, *2* (15), 5352−5357.
(57) Sun, J.; Li, X.; Zhao, Q.; Tadé, M. O.; Liu, S. Construction of p-n Heterojunction *β*-Bi2O3/BiVO4 Nanocomposite with Improved Photoinduced Charge Transfer Property and Enhanced Activity in Degradation of ortho-Dichlorobenzene. *Appl. Catal., B* **2017**, *219*, 259−268.
(58) Cao, J.; Xu, B.; Lin, H.; Luo, B.; Chen, S. Chemical etching preparation of BiOI/BiOBr heterostructures with enhanced photocatalytic properties for organic dye removal. *Chem. Eng. J.* **2012**, *185−186*, 91−99.
(59) Wen, X.-J.; Niu, C.-G.; Zhang, L.; Liang, C.; Zeng, G.-M. An in depth mechanism insight of the degradation of multiple refractory pollutants via a novel SrTiO3/BiOI heterojunction photocatalysts. *J. Catal.* **2017**, *356*, 283−299.
(60) Jiang, D.; Chen, L.; Zhu, J.; Chen, M.; Shi, W.; Xie, J. Novel p-n heterojunction photocatalyst constructed by porous graphite-like C3N4 and nanostructured BiOI: facile synthesis and enhanced photocatalytic activity. *Dalton T* **2013**, *42* (44), 15726−34.
(61) Lu, H.; Hao, Q.; Chen, T.; Zhang, L.; Chen, D.; Ma, C.; Yao, W.; Zhu, Y. A high-performance Bi2O3/Bi2SiO5 p-n heterojunction photocatalyst induced by phase transition of Bi2O3. *Appl. Catal., B* **2018**, *237*, 59−67.
(62) Chen, S.; Hu, Y.; Jiang, X.; Meng, S.; Fu, X. Fabrication and characterization of novel Z-scheme photocatalyst WO3/g-C3N4 with high efficient visible light photocatalytic activity. *Mater. Chem. Phys.* **2015**, *149−150*, 512−521.
(63) Li, J.; Liu, X.; Piao, X.; Sun, Z.; Pan, L. Novel carbon sphere@Bi2MoO6 core−shell structure for efficient visible light photocatalysis. *RSC Adv.* **2015**, *5* (21), 16592−16597.

DOI: 10.1021/acssuschemeng.8b03480
ACS Sustainable Chem. Eng. XXXX, XXX, XXX−XXX